PCCP

COMMUNICATION

View Article Online
View Journal | View Issue

Cite this: *Phys. Chem. Chem. Phys.*, 2024, **26**, 25762

Received 3rd July 2024,
Accepted 25th September 2024

DOI: 10.1039/d4cp02647k

rsc.li/pccp

From weak to strong interactions between halogen and noble gas atoms in halonium complexes†

Wiktor Zierkiewicz, *[a] Steve Scheiner [b] and Mariusz Michalczyk *[a]

Halonium cations can interact through a halogen bond with individual noble gas atoms. These bonds can vary widely in strength from 1 to 25 kcal mol^{-1}. Quantum chemical analyses consider X to be attached to a propyl group, pyridine N, or Xe atom, with X = Cl, Br, and I, interacting with Ar, Kr, and Xe atoms. The most weakly bound dyads are bound primarily by electrostatics, but charge transfer takes a larger role for the more tightly held complexes.

Molecular ions are essential to a great number of reactions, especially when it comes to atmospheric and interstellar chemistry.[1–6] Their highly reactive nature hampers the experimental observation of these entities; however the formation of the halonium ion – 1,3-dibromopropane (DBP^+) cation has been recently investigated by the megaelectronvolt ultrafast electron diffraction (MeV-UED)[7] procedure. The literature offers evidence of other molecular ions such as BH_4^+ or CH_4^{2+}.[8,9] Additionally, these cations were confirmed to pair with noble atom gases, thereby yielding hypercoordinated species.[8,9] For the CH_4^{2+} cation, it was the first time where such fluxional tandem with a noble gas was reported.[8] Analogous systems were considered very recently by a collection of computational methods.[10] BeH_3Ng^+ complexes (Ng = He, Ne, Ar, Kr, Xe, Rn) have been examined by high-level calculations and the Be···Ng interaction was described as mostly electrostatic with a modest share of covalent character. However, previous work has left unresolved a thorough understanding of the bonding within these entities. The current literature involving halonium cations and associated compounds describes the interaction of halonium with two Lewis bases based on different formalisms, recognizing mainly the dominant influence of orbital interactions and electrostatics[11–17] on one hand, or a delocalized molecular orbital scheme[18] on the other. Halonium systems have also been obtained in crystal forms. Our latest survey of the Cambridge Structural Database provides 57 structures containing a halonium cation within the context of X–pyridine$^+$ species (X = F, Cl, Br, I) of formal charge +1 with the X atom bonded to 2 atoms.

The noble gases are commonly known from their non-reactive reputation, as in their neutral atomic state they fulfil the electron octet rule. However, in the last decade there has been study of the so-called "aerogen bond" wherein the noble gas atom is directly involved in a noncovalent bond with one Lewis base or another.[19–25] This bonding is usually facilitated by a σ-hole, a region of reduced electron density, thus signifying a region of positive potential.[26–30] This area is vulnerable to nucleophilic attack and is a common feature of elements of many groups including halogens, chalcogens, pnicogens and even noble gases.[29,31–34] Such bonding is possible even if the Lewis acid is anionic, which is favored by counterions and polar solvents.[35] In a practical sense, the Xe atom was used as part of the functionalized tip in Kelvin probe force microscopy to elucidate the anisotropic charge distribution on halogen atoms, a foundation of the aforementioned σ-hole bonds.[36] Consequently, noble gas atoms' formal unreactivity does not exclude their utility in a variety of contemporary chemical applications.

The current state of affairs leads naturally to the question as to whether a halonium species can engage in a bonding interaction with a noble gas atom. If so, would the resulting complex be the result of a σ-hole on the halonium, or would some other mechanism be responsible. What might be the strength of any such bonding arrangement, and how would this bonding be affected by the nature of the Ng atom, or the halogen to which it is attracted, as well as the remainder of the halonium ion, which is attached to the halogen. The possibility of such a halonium–aerogen interaction to our knowledge has not been tested in the literature as yet. Both halonium and noble gas species are currently of major scientific interest and are significant in atmospheric chemistry. Examining these ephemeral and as-yet-undisclosed species can help us understand the ion chemistry of noble gases more broadly.

[a] *Faculty of Chemistry, Wrocław University of Science and Technology, Wybrzeże Wyspiańskiego 27, 50-370 Wrocław, Poland.*
E-mail: wiktor.zierkiewicz@pwr.edu.pl, mariusz.michalczyk@pwr.edu.pl
[b] *Department of Chemistry and Biochemistry Utah State University Logan Utah, 84322-0300, USA*

† Electronic supplementary information (ESI) available: coordinates of investigated systems, structural and energetic data, and additional computational results. See DOI: https://doi.org/10.1039/d4cp02647k

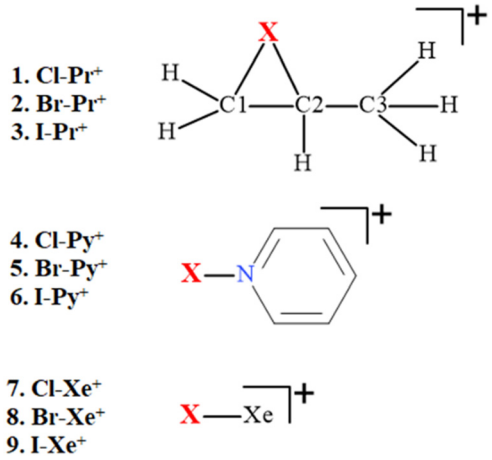

Scheme 1 Representation of monomers where X = Cl, Br, I; Pr = propyl and Py = pyridyl.

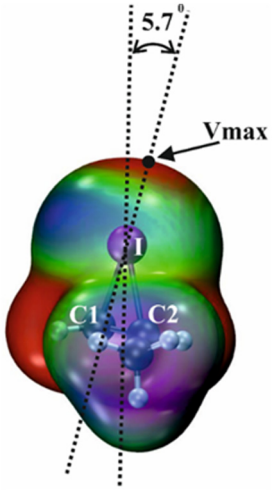

Fig. 1 The MEP visualization for the I–Pr$^+$ halonium monomer. Color scale ranges from 94 (blue) to 120 (red) kcal mol^{-1}.

Three different types of cationic subunits involving halogen atoms were chosen for this project. Scheme 1 depicts the X–Pr$^+$, X–Py$^+$ and X–Xe$^+$ cations and their numeric labelling where X = Cl, Br, and I. Py refers to pyridine and Pr to the propyl entity wherein X is connected to two of the C atoms. The geometrical details of the monomer structures are summarized in Table S1 (ESI†), following full geometry optimization at the M06-2X/def2TZVPP[37–39] level of theory. The two C–X bond lengths in X–Pr$^+$ are not quite equal, and (C1–X) is taken to be the shorter of the two. In all cases the bonds to X elongate as the X atom grows larger.

Analysis of the molecular electrostatic potential (MEP) surrounding each subunit has proven useful in understanding certain aspects of noncovalent interactions.[40,41] The maximum of the MEP on an 0.001 a.u. isodensity surface for each monomer is collected in Table S2 (ESI†). Large positive values greater than 100 kcal mol^{-1} are expected in light of the overall positive charge on each species. $V_{s,max}$ spans the range between 114.2 and 169.2 kcal mol^{-1} increasing as the X atom grows larger: Cl < Br < I. The X–Xe$^+$ monomers have the largest $V_{s,max}$ by around 25–35 kcal mol^{-1}. The disposition of the MEP around the entire monomer is illustrated in Fig. S1 (ESI†), where the red regions indicate the σ-hole positions. To place these quantities in perspective, $V_{s,max}$ for the neutral FX molecules are notably smaller: 41.8, 50.6 and 60.7 kcal mol^{-1}, for FCl, FBr and FI monomers, respectively. Results similar to ours were obtained very recently by Borocci *et al.* for the series of NgHNg$^+$ systems (Ng = He, Ne, Ar) where the σ-hole depth was as high as 259 kcal mol^{-1} for HeHHe$^+$.[42]

In the case of X–Py$^+$ and X–Xe$^+$ the σ-hole lies directly along the extension of the X–N and X–Xe covalent bond axes, respectively, as expected. However, a subtle anomaly appears for the X–Pr$^+$ species. As can be seen in Fig. 1 for I–Pr$^+$, $V_{s,max}$ lies roughly along the line connecting I with the C–C midpoint, rather than either C–I axis. More precisely, this line deviates some 5.7° from the line connecting I with $V_{s,max}$. The data in Table S3 (ESI†) show how this deviation rises to 9.3° for Br–Pr$^+$ and then up to 22.3° for Cl–Pr$^+$. In fact, the maximum position shifts progressively closer to the C1-X angle, from 166.7° for I up to 179.0° for Cl. The final column of Table S3 (ESI†) shows that $V_{s,max}$ lies within 2° of the plane comprised of the C1, C2, and X atoms.

27 different dyads were considered wherein each of the 9 monomers was allowed to interact with a rare gas atom Ng (Ng = Ar, Kr, Xe). The optimized structures of several representative dimers are presented in Fig. S2 (ESI†). The geometrical parameters are listed in Table S4 (ESI†), followed by Table S5 (ESI†) which contains several of the key QTAIM[43,44] and NBO[45] indicators of bond strength. The X···Ng distances elongate along with the Ng atomic size Ar < Kr < Xe. One can observe also a strong tendency for this distance to be reduced from X–Pr$^+$ to X–Py$^+$ and then to X–Xe$^+$, which contains the shortest contacts. The Xe atom lies within a degree of the N–X or Xe–X axis for X–Py$^+$ and X–Xe$^+$. Similar LB···X···LB angles in various halonium compounds were observed elsewhere[17,18] where LB indicates a Lewis base. For the more complicated halogenopropyl cations the location of the noble gas atom adheres closely to the MEP analysis, *i.e.* the position of $V_{s,max}$. For example, in the case of the **3**···Xe complex θ(C1–C2 midpoint)–I–Xe is 175.0°. This angle decreases (*i.e.* less linear) for Br and Cl complexes in the same manner as does $V_{s,max}$. The C1–X···Ng angle is closer to 180° than that for C2, which suggests that the nucleophilic attack is directed more toward the shorter (and stronger) C1–X bond. The location of $V_{s,max}$ *versus* the C1–C2–X plane was also checked for these dimers. The deviation from perfect planarity was calculated to be 0.5 to 2.2° as is evident in Table S3 (ESI†).

Another issue is related to the distortions of the internal geometry caused by complexation with Ng. The internal C1/C2–X, N–X and Xe–X bond lengths are stretched in comparison to their values in isolated monomers. This stretching is noticeably smaller in the case of complexes with X–Pr$^+$ and X–Py$^+$ (from 0.000 to 0.023 Å) than in the [Xe–X···Ng]$^+$ dimers where this elongation varies from 0.03 up to 0.28 Å for the [Xe–Cl···Xe]$^+$ complex. It was observed also that the stretching rises steeply with X: Cl < Br < I, or with Ng: Ar < Kr < Xe.

The interaction energies were computed for each of the 27 dyads, and the results in Tables S5 and S6 (ESI†) subdivide the

complexes into three broad types. E_{int} ranges from −0.8 to −3.3 kcal mol^{-1} for the X–Pr$^+\cdots$Ng dyads, which might categorize them as weak vdW complexes. As in the above properties, the bond strengths increase for heavier noble gases and halogens. The same trend is observed in the [Ng$\cdots$X–Py]$^+$ series where the interaction energies are slightly higher, perhaps landing them in the moderate category. By far, the strongest interactions, with a range between −3.4 and −25.6 kcal mol^{-1} are the Xe–X$^+\cdots$Ng adducts. For the complexes with Ar and Kr atoms as Lewis bases the E_{int} again rises along with X atom size. However, this trend is reversed in complexes with Xe where Xe–Cl$^+$ engages in the strongest binding with E_{int} = −25.56 kcal mol^{-1} and that with Xe–I$^+$ is a bit smaller at −19.87 kcal mol^{-1}. As such, these interactions would be classified as strong ones.

This extreme distinction between X–Pr$^+$ and X–Py$^+$ on one hand, and Xe–X$^+$ on the other, is partially overridden when evaluating the binding energy E_b, which compares the energy of the dyad with the sum of the monomers in their fully optimized geometries. These two quantities thus differ by the deformation energy arising when the two subunits adjust to fit into the complex. This deformation energy E_{def} is listed in Table S6 (ESI†) and is quite small for the X–Pr$^+$ and X–Py$^+$ systems, leaving E_b nearly equal to E_{int}. In the Xe–X$^+$ cases on the other hand, the deformation energies are higher, particularly for the interactions with Xe. E_{def} is the smallest for X=Xe and rises as X becomes smaller to as much as 9.84 kcal mol^{-1} for Xe–Cl$^+$. As a result, the binding energies for the three Xe–X$^+$ complexes with Xe are fairly similar, at 16–17 kcal mol^{-1}.

The presence of a positive charge on the various halonium Lewis acids undoubtedly adds to the strength of the halogen bond. On one end of the broad spectrum of halogen bonds, Ng can in principle interact with a neutral FX molecule. The computed interaction energies listed in Table S7 (ESI†) follow the same trend of becoming more negative for larger X, as well as a heavier Ng atom. However, these neutral XBs are somewhat weaker, lying in the range between 0.6 and 2.6 kcal mol^{-1}, as compared to the 0.8–3.3 kcal mol^{-1} range in Table S5 (ESI†). On the other end of the spectrum would be a bare halogen cation X$^+$, with its concentrated charge acting as a Lewis acid. The removal of the remainder of the cationic species very substantially ramps up the interaction energy to the 26–111 kcal mol^{-1} range. For these bare cations, it is Cl$^+$ that is most strongly bound, and I$^+$ the weakest.

To test the quality of the particular DFT functional, additional calculations were carried out with the much higher level and more accurate CCSD(T) approach[46] to include electron correlation. The results are contained in Table S5 (ESI†) and show only small reductions in the interaction energies for these 27 dyads. Most importantly, all of the M06-2X trends are reproduced by CCSD(T). Given the nature of these systems, it is fair to ask how well a single electronic configuration models the density. An answer to this question arises in the context of the T1 diagnostic that was developed by Lee and Tayor.[47] The values of this parameter are listed in Table S5 (ESI†) for all of the systems considered here. The values of T1 are all comfortably below the 0.05 that has been proposed as an important threshold[48] to gauge the applicability of the single configuration prescription.

QTAIM methodology, which analyzes the topology of the electron density reflects the energetic trends. The values of ρ at the bond critical points are correlated with the interaction energies. For the strongest of the studied complexes, ρ lies between 0.021 and 0.067 a.u., which suggests a certain degree of covalency. For the weakest and intermediate complexes these values occur between 0.007 and 0.017 a.u. Transformation from weak to strong complexes is evident by the values of H (total electron energy density, Table S5, ESI†) at the BCPs. They are positive for the weakest X–Pr$^+\cdots$Ng complexes and negative for the strongest Xe–X$^+\cdots$Ng dyads. Another window into the bonding is provided by NBO analysis, which documented the charge transfer from LP(Ng) to σ*(X–R) orbitals that is characteristic of halogen bonding. Within the X–Pr$^+$ group of adducts both X–C1 and X–C2 orbitals are involved in this manner, with the former more prominent. The strongest [Xe–X$\cdots$Xe]$^+$ complexes led to the highest values of $E^{(2)}$ perturbation energies that amounted to 152 kcal mol^{-1} for X=Cl, almost twice that for X=I (91 kcal mol^{-1}). For X=Br, this $E^{(2)}$ value was roughly 130 kcal mol^{-1}. This fact additionally explains why the [Xe–Cl$\cdots$Xe]$^+$ dimer has a larger interaction energy than the [Xe–Br$\cdots$Xe]$^+$ and [Xe–I$\cdots$Xe]$^+$. The elevated deformation of the chlorine monomer permitted a more suitable orientation of the appropriate orbitals, resulting in a larger interaction energy between Xe–Cl$^+$ and Xe than in the case of the MEP-promoted iodine and bromine monomers.

Examination of the manner in which the electron density shifts when each dyad is formed can add insight into the character of the interaction. These shifts are illustrated in Fig. 2 for the example of the PrI$^+\cdots$Xe complex where increases in density are denoted by blue color while the red regions indicated depletion. The largest shifts

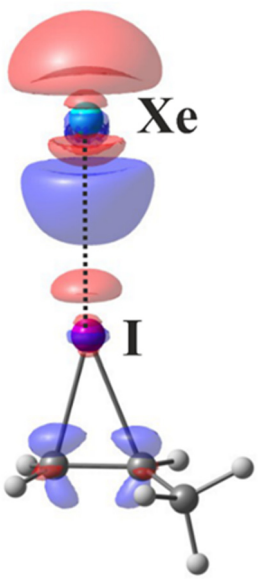

Fig. 2 Electron density difference diagram for the Xe$\cdots$I–Pr$^+$ dimer. The blue lobes correspond to accumulation of density while the red lobes represent reduction upon complexation. The electron density isovalue contour corresponds to 0.001 a.u.

occur in the vicinity of Xe, comprising a displacement/polarization toward the bonding region midway along the Xe···I axis.

The way in which the various prime physical components combine to form the complexes was examined by ALMO-EDA decomposition of the total interaction energy.[49,50] One advantage of this particular method, which distinguishes it from many other decomposition approaches in the literature, is its ability to separate charge transfer from polarization contributions. The absolute values of the derived components are listed in Table S8 (ESI†), along with their percentage contribution to the total attractive energetics. Starting with the Ar systems, electrostatics comprise roughly 50% of this total for PrB^+, $PrCl^+$, $PyCl^+$ and $PyBr^+$. But this percentage diminishes to roughly 20% when X=I, or for the various X–Xe^+ species. On the other hand, ELEC makes up about 20% for all complexes when bound to Xe. Dispersion is quite variable, accounting for between 9% and 35%, generally largest for X=I. Charge transfer is generally largest for X=I, and is especially large for the Xe–X^+ systems, where it can rise to as much as 55 kcal mol^{-1}. The contribution of polarization energy is smaller but also appreciable, in the 9–24% range. One might conclude that the composition of forces is rather sensitive to changes from one system to the next. In general, electrostatics are most impactful for the weakest complexes, but stronger dimers are stabilized by a mix of dispersion and charge transfer; the strongest complexes rely to a large degree on charge transfer. Further investigation of the nature of these halonium complexes was conducted by means of natural resonance theory (NRT), which is incorporated into the NBO protocol, and which can help distinguish between covalent and ionic character. The percentage contributions of these two aspects are exhibited in Table S9 (ESI†) and show a conversion from ionic to covalent as the complex becomes more stable and more saturated by the charge transfer influence. For the $[Xe–X\cdots Ng]^+$ dyads the covalency grows from only 20% in Xe–I···Ar^+ (for which E_{int} = −5.90 kcal mol^{-1}) to 70% for the most stable (−25.6 kcal mol^{-1}) Xe–Cl–Xe^+. Within the two weakest groups, the covalent impact is no more than 10%. An even lower percentage of covalency, less than 5%, was noted for weak complexes with the neutral FX molecule (Table S9, ESI†). On the other hand, the covalency percentage for adducts with X^+ is between 10 and 20 percentage points higher than for complexes with $[Ng–X]^+$. In general, the covalency contribution in the X···Ng^+ dimers diminishes from chlorine to iodine.

In summary, the results presented here document for the first time the stabilizing interaction between halonium systems and a noble gas atom. The bond strengths vary over a wide range from less than 1 to more than 25 kcal mol^{-1}, from vdW to covalent bonding. The weaker complexes contain a major contribution from electrostatics, but this emphasis shifts toward charge transfer for the stronger bonds. The position of the σ-hole is unusual for the propyl haloniums, intermediate between the extensions of the two C–X bonds. The most weakly bonded dyads are roughly 90% ionic, whereas the covalent contribution creeps up to as high as 70% as the bonding strengthens. As a future extension of these results, it would be intriguing to examine how the attachment of the noble gas atoms alters the spectroscopic properties of these ions.

Data availability

The data supporting this article has been included as part of the ESI.†

Conflicts of interest

There are no conflicts to declare.

Acknowledgements

W. Z. and M. M. gratefully acknowledge Polish high-performance computing infrastructure PLGrid (HPC Centers: ACK Cyfronet AGH) for providing computer facilities and support within computational grant no. PLG/2023/016853, Wrocław Center for Networking and Supercomputing (WCSS). This material is also based upon work supported by the U.S. National Science Foundation under Grant No. 1954310 to S. S. This work was financed in part by a statutory activity subsidy from the Polish Ministry of Science and Higher Education for the Faculty of Chemistry of Wroclaw University of Science and Technology.

Notes and references

1 M. Hayyan, M. A. Hashim and I. M. AlNashef, *Chem. Rev.*, 2016, **116**, 3029–3085.
2 D. S. Belic, X. Urbain and P. Defrance, *Phys. Rev. A: At., Mol., Opt. Phys.*, 2015, **91**, 012703.
3 C. D. Hubbard, P. Illner and R. van Eldik, *Chem. Soc. Rev.*, 2011, **40**, 272–290.
4 T. P. Snow and V. M. Bierbaum, *Annu. Rev. Anal. Chem.*, 2008, **1**, 229–259.
5 Q. B. Lu and L. Sanche, *Phys. Rev. Lett.*, 2001, **87**, 078501.
6 D. Smith, *Chem. Rev.*, 1992, **92**, 1473–1485.
7 J. Heo, D. Kim, A. Segalina, H. Ki, D. S. Ahn, S. Lee, J. Kim, Y. Cha, K. W. Lee, J. Yang, J. P. F. Nunes, X. Wang and H. Ihee, *Nature*, 2024, **625**, 710–714.
8 A. Vasquez-Espinal and R. Pino-Rios, *Phys. Chem. Chem. Phys.*, 2023, **25**, 27468–27474.
9 R. Pino-Rios, A. Vasquez-Espinal, S. Pan, E. Cerpa, W. Tiznado and G. Merino, *ChemPhysChem*, 2023, **24**, e202200601.
10 A. Vasquez-Espinal and R. Pino-Rios, *Phys. Chem. Chem. Phys.*, 2024, **26**, 16687–16692.
11 H. Razmazma and A. Ebrahimi, *J. Mol. Graphics Modell.*, 2018, **84**, 134–144.
12 S. B. Hakkert and M. Erdélyi, *J. Phys. Org. Chem.*, 2015, **28**, 226–233.
13 A. Karim, M. Reitti, A. C. C. Carlsson, J. Gräfenstein and M. Erdélyi, *Chem. Sci.*, 2014, **5**, 3226–3233.
14 D. C. Georgiou, P. Butler, E. C. Browne, D. J. D. Wilson and J. L. Dutton, *Aust. J. Chem.*, 2013, **66**, 1179–1188.

15 A. C. C. Carlsson, J. Gräfenstein, A. Budnjo, J. L. Laurila, J. Bergquist, A. Karim, R. Kleinmaier, U. Brath and M. Erdélyi, *J. Am. Chem. Soc.*, 2012, **134**, 5706–5715.
16 P. Ramasami and J. S. Murray, *J. Mol. Model.*, 2024, **30**, 81.
17 L. H. E. Wieske and M. Erdelyi, *J. Am. Chem. Soc.*, 2024, **146**, 3–18.
18 J. D. Velasquez, J. Echeverria and S. Alvarez, *Inorg. Chem.*, 2023, **62**, 8980–8992.
19 A. Bauzá and A. Frontera, *Angew. Chem., Int. Ed.*, 2015, **54**, 7340–7343.
20 M. D. Esrafili and F. Mohammadian-Sabet, *Chem. Phys. Lett.*, 2017, **667**, 337–344.
21 M. D. Esrafili, F. Mohammadian-Sabet and M. Solimannejad, *Chem. Phys. Lett.*, 2016, **659**, 196–202.
22 A. Frontera and A. Bauza, *Phys. Chem. Chem. Phys.*, 2017, **19**, 30063–30068.
23 R. Wang, H. Liu, Q. Li and S. Scheiner, *Phys. Chem. Chem. Phys.*, 2020, **22**, 4115–4121.
24 R. J. Wang, Z. Wang, X. F. Yu and Q. Z. Li, *ChemPhysChem*, 2020, **21**, 2426–2431.
25 W. Zierkiewicz, M. Michalczyk and S. Scheiner, *Phys. Chem. Chem. Phys.*, 2018, **20**, 4676–4687.
26 J. S. Murray and P. Politzer, *WIREs Comput. Mol. Sci.*, 2017, **7**, e13260.
27 P. Politzer and J. S. Murray, *Crystals*, 2017, **7**, 212.
28 P. Politzer, J. S. Murray, T. Clark and G. Resnati, *Phys. Chem. Chem. Phys.*, 2017, **19**, 32166–32178.
29 T. Clark, M. Hennemann, J. S. Murray and P. Politzer, *J. Mol. Model.*, 2007, **13**, 291–296.
30 P. Politzer, P. Lane, M. C. Concha, Y. G. Ma and J. S. Murray, *J. Mol. Model.*, 2007, **13**, 305–311.
31 J. S. Murray, P. Lane and P. Politzer, *J. Mol. Model.*, 2009, **15**, 723–729.
32 S. Burguera, R. M. Gomila, A. Bauzá and A. Frontera, *Inorganics*, 2023, **11**, 209.
33 G. Resnati, P. Scilabra and G. Terraneo, *Acta Crystallogr., Sect. A: Found. Crystallogr.*, 2019, **75**, E488.
34 A. Bauza, T. J. Mooibroek and A. Frontera, *ChemPhysChem*, 2015, **16**, 2496–2517.
35 A. Grabarz, M. Michalczyk, W. Zierkiewicz and S. Scheiner, *Molecules*, 2021, **26**, 2116.
36 B. Mallada, A. Gallardo, M. Lamanec, B. de la Torre, V. Spirko, P. Hobza and P. Jelinek, *Science*, 2021, **374**, 863–867.
37 Y. Zhao and D. G. Truhlar, *Theor. Chem. Acc.*, 2008, **120**, 215–241.
38 F. Weigend and R. Ahlrichs, *Phys. Chem. Chem. Phys.*, 2005, **7**, 3297–3305.
39 F. Weigend, *Phys. Chem. Chem. Phys.*, 2006, **8**, 1057–1065.
40 P. Politzer and J. S. Murray, *Theor. Chem. Acc.*, 2021, **140**, 7.
41 J. S. Murray and P. Politzer, *WIREs Comput. Mol. Sci.*, 2011, **1**, 153–163.
42 S. Borocci, F. Grandinetti and N. Sanna, *Chem. Phys. Lett.*, 2023, **819**, 140443.
43 R. F. W. Bader and H. Essen, *J. Chem. Phys.*, 1984, **80**, 1943–1960.
44 R. Bader, *Atoms In Molecules. A Quantum Theory*, Clarendon Press, Oxford, 1990.
45 F. Weinhold, C. R. Landis and E. D. Glendening, *Int. Rev. Phys. Chem.*, 2016, **35**, 399–440.
46 K. Raghavachari, G. W. Trucks, J. A. Pople and M. Headgordon, *Chem. Phys. Lett.*, 1989, **157**, 479–483.
47 T. J. Lee and P. R. Taylor, *Int. J. Quantum Chem.*, 1989, **36**, 199–207.
48 A. Obeng and J. Autschbach, *J. Chem. Theory Comput.*, 2024, **20**, 4965–4976.
49 P. R. Horn, Y. Mao and M. Head-Gordon, *Phys. Chem. Chem. Phys.*, 2016, **18**, 23067–23079.
50 P. R. Horn, Y. Mao and M. Head-Gordon, *J. Chem. Phys.*, 2016, **144**, 114107.